AAPS PharmSciTech (2022) 23: 114
https://doi.org/10.1208/s12249-022-02259-z

RESEARCH ARTICLE

Characterizing the Effects of Nasal Prong Interfaces on Aerosol Deposition in a Preterm Infant Nasal Model

Karl Bass[1] · Mohammad A. M. Momin[2] · Connor Howe[1] · Ghali Aladwani[1] · Sarah Strickler[1] · Arun V. Kolanjiyil[1] · Michael Hindle[2] · Robert M. DiBlasi[3] · Worth Longest[1]

Received: 18 February 2022 / Accepted: 20 March 2022 / Published online: 19 April 2022
© The Author(s) 2022

Abstract

The objective of this study was to characterize the effects of multiple nasal prong interface configurations on nasal depositional loss of pharmaceutical aerosols in a preterm infant nose-throat (NT) airway model. Benchmark *in vitro* experiments were performed in which a spray-dried powder formulation was delivered to a new preterm NT model with a positive-pressure infant air-jet dry powder inhaler using single- and dual-prong interfaces. These results were used to develop and validate a computational fluid dynamics (CFD) model of aerosol transport and deposition in the NT geometry. The validated CFD model was then used to explore the NT depositional characteristic of multiple prong types and configurations. The CFD model highlighted a turbulent jet effect emanating from the prong(s). Analysis of NT aerosol deposition efficiency curves for a characteristic particle size and delivery flowrate (3 µm and 1.4 L/min (LPM)) revealed little difference in NT aerosol deposition fraction (DF) across the prong insertion depths of 2–5 mm (DF = 16–24%) with the exception of a single prong with 5-mm insertion (DF = 36%). Dual prongs provided a modest reduction in deposition vs. a single aerosol delivery prong at the same flow for insertion depths < 5 mm. The presence of the prongs increased nasal depositional loss by absolute differences in the range of 20–70% compared with existing correlations for ambient aerosols. In conclusion, the use of nasal prongs was shown to have a significant impact on infant NT aerosol depositional loss prompting the need for prong design alterations to improve lung delivery efficiency.

KEY WORDS trans-nasal aerosol delivery · nose-to-lung aerosol delivery · infant DPI · inline DPI · active DPI · high dose DPI · rapid aerosol administration

INTRODUCTION

Trans-nasal or nose-to-lung (N2L) aerosol administration through a nasal prong interface has been demonstrated to be a viable approach for delivering pharmaceutical aerosols to term and preterm infants (1–8). This approach is advantageous during different forms of non-invasive ventilation (NIV) where the aerosol generation source is placed in-line with the gas delivery system and the aerosol passes through the NIV interface to reach the infant. Multiple forms of infant NIV employing nasal prong interfaces include nasal continuous positive airway pressure (nCPAP), nasal intermittent positive airway pressure (NIPPV), and high flow nasal cannula (HFNC) therapy (4, 9). Delivery of high-dose aerosols such as inhaled bronchodilators, antibiotics, or surfactants is often proposed via nasal prong interfaces during NIV as a means to maintain respiratory support during expected long nebulization times (6, 7, 10–12). Alternatively, high-dose aerosols may be delivered directly to infants before, during, or after NIV respiratory support using nasal prong interfaces and rapid dry powder aerosol delivery systems (13–16). For example, Howe *et al.* (13) proposed a direct-to-infant dry powder delivery strategy that employs a single nasal prong interface and administers both a full inhalation breath and aerosol bolus with short (approximately

✉ Worth Longest
pwlongest@vcu.edu

1 Department of Mechanical and Nuclear Engineering, Virginia Commonwealth University, 401 West Main Street, P.O. Box 843015, Richmond, VA, USA

2 Department of Pharmaceutics, Virginia Commonwealth University, 410 North 12 Street, P.O. Box 980533, Richmond, VA 23298-0533, USA

3 Department of Respiratory Care, Seattle Children's Hospital, Seattle, Washington, USA

0.2 s) actuation times. As part of the aerosol delivery strategy implemented in the *in vitro* study of Howe *et al.* (13), the nostril without the nasal prong was held closed during device actuation and then opened to allow for exhalation similar to the infant resuscitation strategy of te Pas *et al.* (17). Using this approach, lung delivery efficiency was on the order of 50% of a loaded 10 mg powder dose based on *in vitro* experiments with a realistic nose-throat (NT) model of a term newborn infant and open filter system (13). In human subjects, N2L administration of high-dose pharmaceutical aerosols through nasal prong interfaces has progressed to clinical testing (3, 7, 11, 12), largely focused on the administration of nebulized liquid surfactants combined with NIV (i.e., nCPAP).

A number of studies have characterized the deposition of nasally inhaled aerosols in infants using realistic *in vitro* replicas (18–24) and computational fluid dynamics (CFD) models (25, 26) in the absence of a nasal interface, i.e., for ambient or environmentally inhaled aerosols. Nasal deposition of environmentally inhaled aerosols has been characterized for infants in the age ranges of 0–3 months (21, 22) and 3–18 months (19, 20). CFD studies have characterized progression of nasal deposition with age starting with full-term newborn infants (25, 27). These studies typically highlight high intersubject variability in nasal depositional loss of aerosol, which persists even when deposition fractions are plotted against the traditional impaction parameter of d_a^2Q, where d_a is the particle or droplet mean aerodynamic diameter (often in μm) and Q is the inhalation flowrate (often in cm^3/s or LPM). Variability in nasal deposition fraction curves is typically collapsed when plotted against combinations of nondimensional Reynolds (Re) and Stokes (Stk) numbers, and in some cases, the Euler number, with a characteristic length scale represented as $D_{V/SA}$, which is calculated as the nasal cavity volume (V) divided by the surface area (SA). *In vitro* and some CFD studies have highlighted a simpler pressure-based approach that is also effective for collapsing the deposition data to a single curve (22, 28, 29).

Few previous studies have characterized nasal deposition for preterm infants (30, 31), likely due to the rarity of preterm airway models. Clark *et al.* (30) recently determined the aerosol deposition curve in an *in vitro* nasal airway model developed from a preterm infant (DiBlasi preterm nasal model) (32) using environmentally inhaled droplets (i.e., without a nasal interface). Clark *et al.* (30) highlighted that nasal deposition in the preterm model was lower than deposition in a nasal model from a 4-year-old and similar to the 9-month-old SAINT nasal model (33), each evaluated with age-appropriate inhalation conditions for environmentally inhaled aerosols. Lower nasal depositional loss in the preterm model was unexpected and postulated to be due to high intersubject variability (30). However, a review of published preterm and infant nasal models (25–27, 31) indicates that the nasal meatus structures and curved turbinate flow passages develop and become more pronounced with age and are typically not fully formed in preterm infants. As a result, preterm nasal airways may have an overall simpler structure than occur with full-term infants, thereby potentially increasing aerosol transmission at typical or age-appropriate inhalation conditions. As such, the low lung deposition observed in these preterm infant models is more likely related to low lung volumes and fast breathing rates of preterm babies.

Multiple *in vitro* (1, 4–6, 8, 16, 34), *in vivo* (3, 8, 10, 35, 36), and CFD (37) studies have considered infant nasal aerosol deposition and lung transmission with the inclusion of nasal prong interfaces for realistic polydisperse pharmaceutical aerosols. For example, Corcoran *et al.* (3) recently reported the *in vivo* nasal deposition and lung delivery efficiency of vibrating-mesh nebulized aerosol delivered to 18 infants through a non-occlusive HFNC interface. Due to high delivery system, interface, and nasal depositional losses, average lung deposition efficiency was only 0.46% of the nebulized dose at a typical 2 LPM gas flowrate, which was required to provide simultaneous respiratory support. Sunbul *et al.* (4) implemented the DiBlasi preterm nasal model to assess lung transmission efficiency of vibrating-mesh nebulized pharmaceutical aerosol for multiple NIV systems (HFNC, bubble CPAP, SiPAP). Best-case lung delivery efficiencies among different nebulizer placement positions were < 2% of the nebulized dose across all systems considered. Bianco *et al.* (34) recently showed 10 to 20% estimated lung deposition when applying continuous high-dose aerosolized surfactant with eFlow Neos nebulizer through 8 different bi-nasal short prongs affixed to a preterm NT airway (PrINT) during simulated pre-term infant breathing and nasal CPAP. For the dry powder air-jet delivery system of Howe *et al.* (13) with a single-prong nasal interface, nasal depositional loss of an aerosol with a 1.7 μm MMAD delivered at 2.7 LPM was approximately 20%, and when considered with other losses, resulted in a tracheal filter delivery efficiency of approximately 50% of the inhaler loaded powder dose.

Considering the previous literature, studies that include infant nasal interfaces, typically combined with NIV, tend to predict lower lung deposition efficiencies than would be expected from deposition efficiency curves generated with environmentally inhaled aerosols. As demonstrated in numerous studies, including some of our own, low lung delivery efficiency of nasally administered aerosols is in part due to high depositional losses in the interface (38). Furthermore, as with other modes of pharmaceutical aerosol delivery such as oral inhalation with dry powder inhalers (DPIs) (39–42), the nasal prong interface is also expected to have an impact on deposition in the nasal region. This impact may be especially enhanced in the already small and

narrow airways of preterm infants. For example, the nostril hydraulic diameter of a preterm infant may be approximately 4.5 mm. If nasal prong wall thickness is 1 mm, then the available diameter for airflow passage is reduced (by 1 mm on two sides) to 2.5 mm, resulting in a diameter reduction of 1.8-fold. Considering that inlet velocity is inversely proportional to inlet diameter squared, for the same inhalation flowrate, the nostril inlet velocity with the prong included is increased by a factor of 3.2, which likely forms a jet of air entering the infant nose. As with other modes of aerosol drug delivery, such as oral inhalation with DPIs and metered dose inhalers (MDI) (42, 43), air jets induced by the device or patient interface are known to significantly increase depositional loss. Similarly, typical nasal prong length used with NIV is 10–11 mm for a preterm infant (44). If the cannula is inserted approximately 60% of this length, the cannula inlet likely extends approximately 10% through the length of the nasal passage. Furthermore, the cannula may be compressed creating a less stable elongated inlet jet of air, and the inlet jet may impinge on the upper nasal surface.

As described, there is currently a lack of data in the literature on the impact of nasal cannula interfaces on the deposition of pharmaceutical aerosols in the NT region for all ages. This information is especially important for preterm infants, where nasal prong interfaces may have the most significant impact on nasal deposition. Important issues to address include the effect of the expected air jet formed by nasal prong interfaces on net aerosol loss in the nasal cavity. The effect of prong insertion distance needs to be determined for prongs designed for insertion into the nasal airway openings. Furthermore, it is not clear if rapid single-prong aerosol administration (13) results in a net increase or decrease in transmission of aerosol to the lungs. Administering the aerosol through a single-prong interface is convenient for rapid aerosol delivery and helps to more easily form an airtight seal (13). However, a single-prong interface increases flow through one nostril and alters the flow dynamics in the nasopharyngeal region, potentially increasing nasal depositional loss by a significant amount.

The objective of this study was to characterize the effects of multiple nasal prong interface configurations on nasal depositional loss and lung transmission of pharmaceutical aerosols in a preterm infant NT airway model using CFD simulations validated with realistic *in vitro* experiments. Nasal prong configurations included both external and internal designs. External nasal prongs had a cone structure on the outer surface that forms an airtight seal with the nasal wall upon insertion by a few millimeters, as with the aerosol delivery approach developed by Howe *et al.* (13) for direct-to-infant aerosol administration. Internal prongs were similar to current infant NIV interfaces, as with nasal CPAP, and had a straight cylindrical design that forms an airtight seal upon internal insertion, with multiple insertion distances possible. Both single- and dual-prong configurations were evaluated for direct-to-infant and simultaneous aerosol administration during NIV. For assessing preterm nasal deposition, the DiBlasi preterm nasal airway model was implemented, which is based on a 1500 g 28-week gestation neonate, with the addition of age-appropriate pharyngeal and laryngeal regions. Flowrates of 1 to 4 LPM were considered to capture aerosol delivery scenarios occurring with spontaneous respiration during NIV and with direct-to-infant positive pressure aerosol administration. Both *in vitro* and CFD results were used to identify nasal prong interface configurations that can best maximize the lung delivery efficiency of a pharmaceutical aerosol administered using the N2L route.

MATERIALS AND METHODS

To evaluate NT aerosol depositional loss for different patient interface design concepts, two prong types (internal and external), two prong configurations (single and dual), and three insertion depths (2, 5, and 11 mm) were considered. The internal prong type was made from a flexible material that facilitates insertion into the nasal passage, with clinicians typically inserting the prong 2–5 mm into the nares (Fig. 1a). This prong type was evaluated experimentally at 5 mm insertion and with CFD models at the 2, 5, and 11 mm insertion depths. The external prong type was made from a rigid material with an expanding external wedge shape that only permits insertion into the nose a short distance (< 2 mm) but maintains the circular cross-section of the prong outlet (Fig. 1b). The expected advantage of the flexible internal prong type is reduced NT losses from bypassing a portion of the anterior nose, while the expected advantages of the external prong type is lower flow velocities, due to the prong not being compressed to an elliptical cross-section, opening the nostril, and better sealing around the nostril walls. Insertion depths were selected to be representative of typical practice (2 and 5 mm), and the maximum insertion depth that the prong length allows (11 mm). The full insertion case bypasses a significant amount of the nasal passage but significantly compresses the prongs. Finally, the dual-prong configuration tests the traditional gas delivery cannula design where a prong enters each nostril, whereas the single prong transmits flow directly from the DPI to one of the nostrils without dividing the flow stream. The single-prong configuration may reduce losses in the patient interface, as there is less possibility for impaction deposition within the cannula flow bifurcation, but NT losses may be higher as the flow through one side of the nasal passage is doubled compared to the dual-prong configuration. In summary, eight interface cases were considered, and each case was evaluated at 1.85 LPM and 4.00 LPM across 0.41–13.85 μm particle

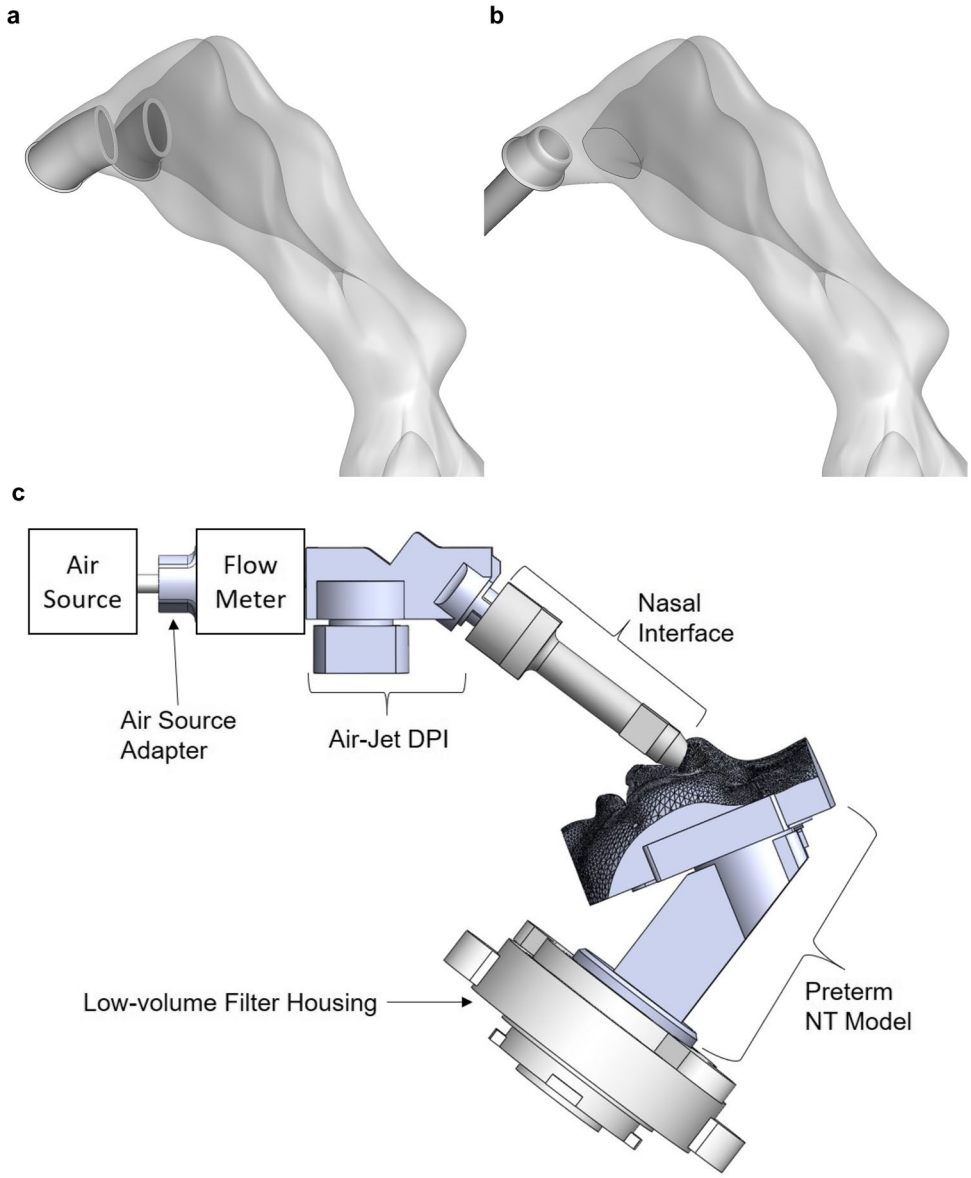

Fig. 1 **a** Dual internal prong with 5 mm insertion and **b** single external prong with 2 mm insertion cases. **c** Overview of aerosol delivery set-up used during *in vitro* testing

aerodynamic diameters, which was sufficient to develop impaction parameter curves and correlations that are predictive of NT loss for each design concept. *In vitro* experiments were conducted for two of the interface cases, which were then used to benchmark the CFD models. Once validated, the CFD model was used to assess all interfaces, flowrates, and aerosol size combinations considered, and to develop the depositional loss correlations.

Nose-Throat Model

The NT model used in the current study was developed from CT scans of a 28-week old preterm infant (1500 g weight) and provided by a co-investigator (RMD) from Seattle Children's Hospital (32). The CT scans did not include the laryngeal region, which is known to be an important component of flow development entering the upper airways (45), but the model did include the entire naso-oropharynx section down to the epiglottis. To form a more complete preterm NT geometry, a laryngeal region and a portion of the trachea were extracted from a 6-month-old NT case (37) and smoothly coupled to the preterm NT to form a full model from nares through the nasal cavity, nasopharynx, larynx, and a section of the trachea. Prior to connection, the larynx was scaled by a factor of 0.6 so that the dimensions were consistent with a 1500-g preterm infant (13). Diameters through the glottis and larynx were measured to be approximately 3–4 mm throughout the cross-section, which is consistent with the 3–7 mm diameter range at 28 weeks gestational age reported by Schild (46). The larynx was located in the preterm NT model such that the glottis was at a similar, but scaled, distance away from the main curvature in the

nasopharynx as the 6-month-old model. Vorperian *et al.* (47) reported that the larynx undergoes its most rapid change in vertical position from 0 to approximately 14 months. However, the difference in laryngeal descent (measured from thyroid notch to the posterior nasal spine) between 0 and 6 months is only 6 mm. Therefore, the scaled positioning on the larynx addition to the preterm NT model was deemed acceptable.

Experimental Materials and Powder Formulation

Albuterol sulfate (AS) USP was purchased from Spectrum Chemicals (Gardena, CA) and Pearlitol® PF-Mannitol was donated from Roquette Pharma (Lestrem, France). Poloxamer 188 (Leutrol F68) was donated from BASF Corporation (Florham Park, NJ). L-leucine and all other reagents were purchased from Sigma Chemical Co. (St. Louis, MO).

As a highly dispersible powder, a single batch of a spray-dried AS excipient enhanced growth (AS-EEG) formulation was produced based on the optimized method described by Son *et al.* (48) using a Büchi Nano spray dryer B-90 HP (Büchi Laboratory-Techniques, Flawil, Switzerland). The model powder formulation contained a 30:48:20:2% w/w ratio of AS, mannitol, l-leucine, and Poloxamer 188. This AS-EEG powder was selected as a model formulation for the benchmark experiments based on readily available methods for direct and accurate quantification. Therapeutics of interest for N2L dry powder aerosol delivery to infants, potentially with high doses, include dry powder surfactants, antibiotics, and non-steroidal anti-inflammatory compounds.

Experimental Methods

The experimental work presented in the current study largely follows the same methods as described by our previous work in the development of aerosolized surfactant delivery systems for preterm infants (13, 49). Briefly, an air-jet DPI is used to aerosolize the powder, which consists of an aerosolization chamber with small diameter inlet/outlet flow pathways (50, 51). As illustrated in Fig. 1c, a positive pressure air source was used to generate 10 mL air bursts through the air-jet DPI. As air passes through the small diameter inlet flow pathway, a high-speed turbulent jet is created within the aerosolization chamber. Secondary velocity currents from this high-speed jet initially fluidize the powder followed by additional breakup in the high-speed jet and aerosol size selection through the outlet flow passage. A nasal interface with a gradual expansion was used to reduce the high-speed aerosol exiting the air-jet DPI with low depositional loss. Further details on the preterm infant aerosol delivery system are reported by Howe *et al.* (13, 49).

In the experiments, the positive pressure air source was a custom-built timer device that incorporated a compressed gas inlet, pressure regulator, miniature solenoid valves, and an electromechanical control unit. The timer device was calibrated to deliver constant gas waveforms containing 10 ml air volumes. Waveform duration was ~ 0.4 s, which is consistent with typical inhalation times of preterm infants (52). Metrics Q_{90} and Q_{99} indicate volumetric flowrates (LPM) for which 90% and 99% of rapidly sampled waveform flowrate measurements fall below. For the timer device settings used in the experiments, Q_{90} and Q_{99} measured values were 1.7 and 1.85 LPM, respectively.

Separate experiments were conducted to evaluate the aerosol size exiting the nasal prong configurations and NT depositional loss. For these bench experiments, the external prong configuration was evaluated for single- and dual-prong cases. In all experiments, 10 mg fill masses of the AS-EEG formulation were loaded into the air-jet DPI. The devices were actuated three times with a 5-s pause between each actuation. To assess the aerosol size distribution that exited the prongs, which served as the input to the CFD models, the nasal prongs were attached to the pre-separator inlet of a Next Generation Impactor (NGI; MSP, Shoreview, MN), as illustrated by Howe *et al.* (13, 49). Co-flow air was pulled around the prong outlet(s) and into the NGI using a downstream vacuum pump, operated at 45 LPM, to ensure that the entire aerosol plume was pulled into the NGI. Each stage of the NGI was coated with MOLYKOTE® 316 silicone spray (Dow Corning, Midland, MN) to minimize powder bounce and re-entrainment. Based on an airflow rate of 45 LPM, the NGI cutoff stages were determined using the formula specified in USP 35 (Chapter 601, Apparatus 5).

In separate experiments, NT deposition and aerosol delivery to a tracheal filter were evaluated in a physical *in vitro* model of the preterm NT. The majority of the NT model was 3D printed in rigid plastic, with the exception of the anterior nose and face, which were cast in silicone to create a flexible and realistic region of the connection with the nasal prongs. A small amount of lubrication oil was applied to the external surface of the prongs to ensure an air-tight seal. For single-prong administration, the contralateral nostril was held closed during delivery and then released after the 5-s breath-hold period. NT model segments were also coated with MOLYKOTE® 316 silicone to prevent particle bounce and re-entrainment. As illustrated in Fig. 1c, the *in vitro* NT model ended with a high-efficiency fiber filter (Pulmoguard II) contained in a custom low air-volume filter holder to minimized dead space.

For both the NGI and airway model studies, after aerosol delivery, the powder formulation masses retained in the air-jet DPI and patient interface, as well as collected on the pre-separator, impaction plates and the filter of the NGI or in the airway model and final filter were recovered by washing with appropriate volumes of deionized water, and the drug content was quantified by high-performance

liquid chromatography (HPLC) assay. The mass of the AS recovered on each collection site was expressed as a percentage of the loaded AS dose for all regions except for the NT loss (see below). In both studies, the system-emitted dose (ED) was calculated by subtracting the mass of the AS retained in the device (air-jet DPI, interface, and prong(s)) from the loaded AS dose. For the NGI study, fine particle fraction of the EEG formulation ($FPF_{<5\ \mu m/ED}$) and sub-micrometer FPF ($FPF_{<1\ \mu m/ED}$) were defined as the mass fraction less than 5 μm and 1 μm, respectively, expressed as a percentage of the ED. MMAD, $FPF_{<5\ \mu m/ED}$, and $FPF_{<1\ \mu m/ED}$ were calculated by linear interpolation using a plot of cumulative percentage drug mass vs. cutoff diameter. For the airway model deposition study, the NT loss (drug deposited in the airway model) was expressed as a percentage of the system-emitted dose for comparison with the CFD results, and the tracheal filter dose was reported as a percentage of the loaded dose to assess overall efficiency.

CFD Models

Computational Domain and Spatial Discretization

The computational domain of the preterm NT model, with each of the aforementioned prong configurations, was discretized into control volumes by utilizing the meshing capabilities in FLUENT v19.3 (ANSYS Inc., Canonsburg, PA). The unstructured polyhedral mesh topology with prismatic near-wall cell layers was used to accurately capture the flow in the near-wall region and resolve the complexity of the nasal cavity surfaces. Our group has published several studies recently that demonstrate the strengths of polyhedral control volumes with prismatic near-wall cells for characteristic geometries (53), the nasal passage of infants (37), diseased upper airways (38), and intermediate airway bifurcations (54).

Mesh independence was established using the Roache method for grid refinement (55) by evaluating the volume-average velocity magnitude (v_{mag}) and turbulent kinetic energy (TKE) across a coarse (2.0-million cells), medium (4.4-million cells), and fine (8.0-million cells) discretization of the single internal cannula type with 2 mm insertion depth (1.85 LPM flowrate). Between the medium and fine meshes, the grid convergence index (GCI) was less than 1% for both v_{mag} and TKE. Therefore, the medium mesh provided acceptable mesh independence and its degree of spatial resolution was applied to all other cases of different prong type, prong configuration, and insertion depth that were evaluated in this study.

Numerical Models and Solver Settings

The CFD setup generally followed our previously established best practices for numerical modelling of pharmaceutical aerosol transport through the nasal cavity (37, 56). Some additional numerical sub-models were also implemented to address specific elements of predicting aerosol loss in a preterm NT model. Specifically, the wall roughness model was activated to represent influences of surface characteristics on the flow and turbulence field in the near-wall region and related effects on particle deposition. As the airways become narrower, when comparing adult and preterm models, the surface roughness becomes more critical and has a greater effect on the flow-field characteristics, especially in the transitional flow regime. Preliminary CFD work showed that using a roughness height of 50 μm gave the best match between numerical and experimental deposition data, which was also consistent with measured surface roughness heights.

For all cases considered in this study, the inlet Reynolds number at the cannula prong was at most approximately 1900 for the single-prong configuration at 4 LPM, which is in the laminar to transitional flow regime. Considering this, the transition of the flow from the cannula to the nasal cavity is expected to induce turbulence in some or all of the cases, and as such, the low-Reynolds number (LRN) k-ω model was used to model the transitional-to-turbulent flow field. The LRN k-ω model implements an eddy viscosity damping coefficient that allows it to provide an accurate representation of the flow field in regions of both low and high levels of turbulence and can capture the transitional-to-turbulent flow regime (57).

The commercial CFD software package FLUENT v19.3 (ANSYS Inc., Canonsburg, PA) was used to obtain numerical solutions for all transport equations. Model settings following our best practices (37, 56), with the addition of including the wall roughness model as stated above. Briefly, all spatial discretizations of flow and transport equations were second-order accurate, the Green-Gauss Node-based method was used for gradient discretization, and SIMPLEC scheme was used for the pressure–velocity coupling. An in-depth discussion on modelling the mass, momentum, and turbulence transport equations in FLUENT for flow through the airways is given by Longest *et al.* (58, 59). All inlets used the mass flow inlet boundary condition, with the mass flowrate set appropriately to achieve either the 1.85 or 4.00 LPM total flowrate. As the preterm NT model only has one outlet at the end of the trachea, the outflow boundary condition was used, such that all flow that enters through the inlet leaves through the outlet. The walls of the NT model used the no-slip shear condition and the wall roughness was implemented with a roughness height of 50 μm and a roughness constant of 0.5 (the default value). Numerical

extensions were added to the computational domain at the inlets and outlets to avoid flow-boundary recirculation and improve solution stability. The length of each extension was five times the hydraulic diameter of the inlet or outlet boundary.

Particle Transport

The particle trajectories through the continuous phase were calculated with the discrete phase model (DPM) in FLUENT v19.3 with the Runge–Kutta scheme implemented to integrate the equations of motion. The settings for the DPM followed our previously validated best practices for aerosol transport through the nasal cavity (37, 56, 58, 60). The gravity angle was defined such that the NT model was representative of the patient being in the supine position, which is consistent with envisioned clinical practice and the experimental testing for this study. User-defined functions (UDFs) were implemented that correct the particle trajectory in the near-wall region, to account for flow phenomena that is not well captured by the LRN k-ω model. Specifically, these UDFs interpolate field quantities from the computational cell-centroid to the particle location, include anisotropic turbulence fluctuations, and damp the wall-normal velocity to model particle–wall hydrodynamic interactions within the region of 1–2 μm from the wall. Previous studies from our group (37, 56, 58) have shown that these corrections provide a significantly improved validation of CFD models vs. experimental deposition data when compared with the standard particle trajectory calculations, which tend to over-predict aerosol deposition in turbulent and transitional flow regions. Despite hygroscopic excipients being included in the powder formulation, aerosol growth from absorption of moisture from the humid airways was neglected from the CFD model due to the low residence times of particle transport through the nasal cavity. Finally, preliminary work showed that some particles were airborne in the continuous phase of the computational domain (nasal cavity) after the 0.2-s flow actuation. Therefore, particles that were still suspended after 0.2-s flow time (i.e., did not deposit on a wall or leave through the outlet) were assumed to eventually deposit due to their near-wall proximity combined with sedimentation and potential electrostatic attraction forces.

The spatial distribution of the particles as they enter the computational domain followed a blunt velocity profile (1/7th-power law) over the circular prong inlet, which is consistent with the transitional-to-turbulent flow regime. The initial velocity of each particle was dependent on its spatial location and also followed the blunt velocity profile. The aerodynamic particle size distribution followed the NGI cut-off diameters when operated at 45 LPM, which allowed for direct comparison with experimental data, specifically 0.41, 0.65, 1.09, 1.90, 3.26, 5.18, 9.41, and 13.85 μm. The eight bin sizes and two flowrates also provided 16 data points, which were sufficient to develop the non-linear impaction parameter curves. Particle convergence was acceptable with 10,000 particles per bin, which gave a total of 80,000 particles tracked through the domain. This is consistent with the convergence criteria of other studies from our group (54, 61).

RESULTS

Experimental Device Performance and Preterm Nose-Throat Loss

Table I summarizes the experimentally determined aerosolization performance of the single and dual internal prong configurations at an insertion depth of 5 mm in terms of emitted dose, NT losses, expected lung dose, and aerosol size exiting the prong. Results are consistent with the findings of Howe *et al.* (49), who tested similar devices in a 6-month-old NT model that was scaled to preterm dimensions, as opposed to the current study where the nasal model was developed from the anatomy of a preterm infant at a gestational age of 28 weeks. The dual-prong configuration

Table I Summary of Experimentally (*in vitro*) Determined Aerosol Deposition and Size Characterization for Single- and Dual Internal Prong Configurations at an Insertion Depth of 5 mm. Experimental Results are Given as Mean Values with Standard Deviations (SD) shown in Parenthesis ($n=3$)

	Single prong	Dual prong
Aerosol deposition		
DPI retention [%]	25.0 (3.3)	35.7 (1.0)*
Interface DF [%]	11.4 (0.2)	9.7 (1.3)
System ED [%]	63.7 (3.5)	54.6 (1.1)*
NT loss [%][a]	25.2 (3.7)	34.0 (6.0)*
Lung dose [%][b]	43.3 (2.1)	34.1 (0.9)*
Aerosol size		
MMAD [μm]	1.90 (0.10)	2.63 (0.12)*
FPF(< 1 μm/ED) [%]	14.3 (0.5)	3.5 (0.2)*
FPF(< 5 μm/ED) [%]	86.2 (3.1)	59.6 (1.9)*

DPI, dry powder inhaler; *DF*, deposition fraction; *ED*, emitted dose; *NT*, nose-throat; *MMAD*, mass-median aerodynamic diameter; *FPF*, fine particle fraction

[a]NT loss is given as the percentage of mass deposition in the preterm NT model divided by the system emitted dose for direct comparison with CFD models, which do not include the device and patient interface in this study

[b]Lung dose is given as percentage of inhaler loaded dose to clearly demonstrate how much aerosol from the device is capable of navigating the upper airways

*$p<0.05$; paired *t*-test; significant decrease in performance from single to dual-prong configuration

had lower efficiency (p-value < 0.05) than the single-prong device in all performance metrics, except for losses in the patient interface. Delivery system and extrathoracic losses are higher for the dual-prong configuration than with the single prong, producing a mean (SD) system ED of 54.6% (1.1%) vs. 63.7% (3.5%) and NT loss of 34.0% (6.0%) vs. 25.2% (3.7%), respectively. Hence, the single-prong configuration delivers an absolute difference of 9.2% more dose to the lungs or a relative change of 27.0% (34.1% (0.9%) dual vs. 43.3% (2.1%) single). Note that NT loss is given as a percentage of system-emitted dose (exiting the prongs) and all other percentages are expressed relative to the loaded dose.

The reduced performance of the dual-prong configuration is likely a consequence of DPI design instead of cannula efficiency. The dual-prong device has two outlets from the aerosolization chamber that deliver aerosol to the separate prongs, and this design showed reduced performance in aerosolizing the powder bed with an increased MMAD exiting the prongs (Table I; 2.63 μm vs. 1.90 μm). The larger aerosol size is also described by both the FPF (< 1 μm) and FPF (< 5 μm) metrics for the dual-prong configuration (Table I). The increased particle diameter of the aerosol leaving the aerosolization chamber likely explains the increased system and NT losses in Table I as there is more impaction depositional loss. Subsequent sections of this NT characterization study will explore whether the dual-prong configuration with a smaller aerosol size can improve the expected lung dose through the use of CFD analysis.

CFD Model Validation

Comparisons between CFD-predicted and experimentally tested NT loss are presented in Fig. 2 for the single (Fig. 2a) and dual (Fig. 2b) internal prongs at 5-mm insertion depth. For the validation simulations, a steady state gas flowrate of 1.8 LPM was implemented (consistent with the experimental Q_{99} value), which gave the best agreement with the experiments. For both the single- and dual-prong cases, the CFD deposition results are within the standard deviations of the experimental data, which demonstrates validation of the numerical models against *in vitro* testing. Therefore, the methods that were employed for these two models are applied to the other six cases (prong types, configurations, and insertion depths) in subsequent sections of the "Results." From the deposition patterns, it is clear that the majority of loss occurs in the upper region of the NT model as the curvature of the prong directs the flow and aerosol in this direction as it leaves the nasal cannula. This suggests opportunities for design improvements with prongs that direct the aerosol more towards the central path of the nasal passage.

Flow Field Characteristics in Preterm Nose-Throat Model

Figure 3 illustrates streamlines of velocity magnitude in the single internal prong with 11 mm insertion depth (Fig. 3a) and single external prong (Fig. 3b) cases at 1.85 LPM inlet flowrate. Firstly, the streamlines in both examples show how the prong design directs the flow towards the upper region of the NT model, which corroborates the deposition patterns that were presented in Fig. 2. The 11-mm insertion with the flexible internal prong (Fig. 3a) creates a very narrow and elongated outlet, which increases the flow velocity (for a given flowrate) that enters the nasal passage. This leads to jet impingement of the flow on the nasal cavity surfaces and generates a large amount of turbulent kinetic energy (TKE) throughout the flow field (Fig. 3c vs. 3d), which in turn increases the likelihood of impaction depositional losses.

Figure 4 illustrates streamlines, colored by velocity magnitude, for the external prong type using both single

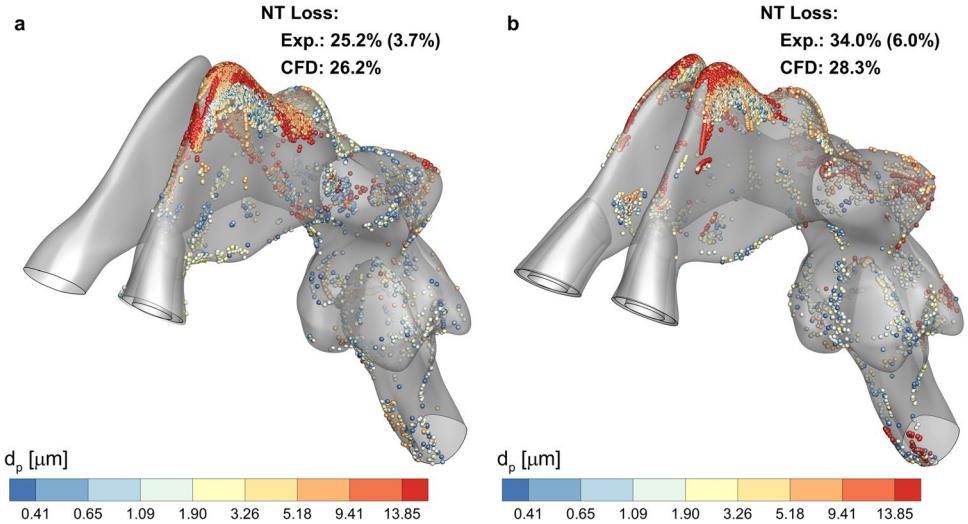

Fig. 2 Validation of computational fluid dynamics (CFD) models compared with experimental data (Exp) for the **a** single and **b** dual internal prong with 5 mm insertion cases at a flow rate of 1.85 LPM (Q_{99} experimental value)

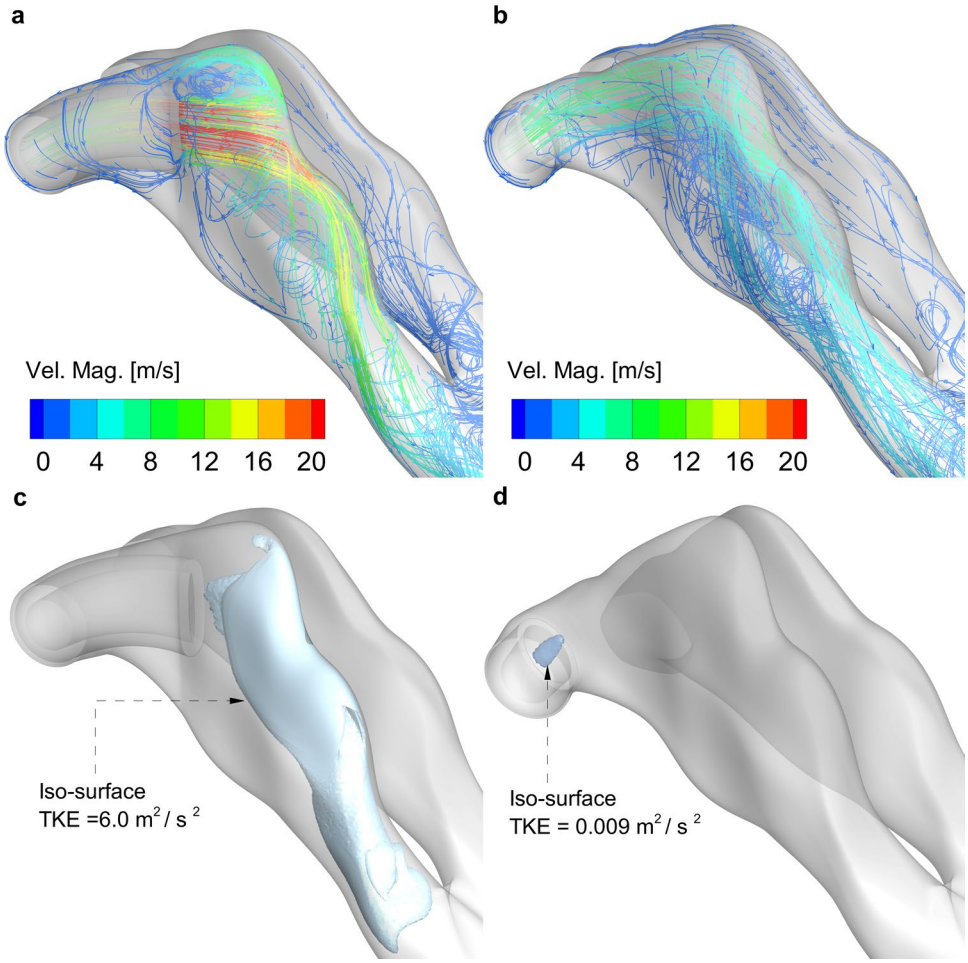

Fig. 3 Comparisons of jet impingement between **a** single internal prong with 11 mm insertion and **b** single external prong with 2 mm insertion cases. Isosurfaces of turbulent kinetic energy (TKE) for the **c** single internal prong with 11 mm insertion and **d** single external prong with 2 mm insertion cases. The narrow elliptical outlet of the compressed internal prong combined with its close proximity to the NT model surface leads to high velocity jet impingent and generation of highly-turbulent flow, which both increase aerosol depositional loss

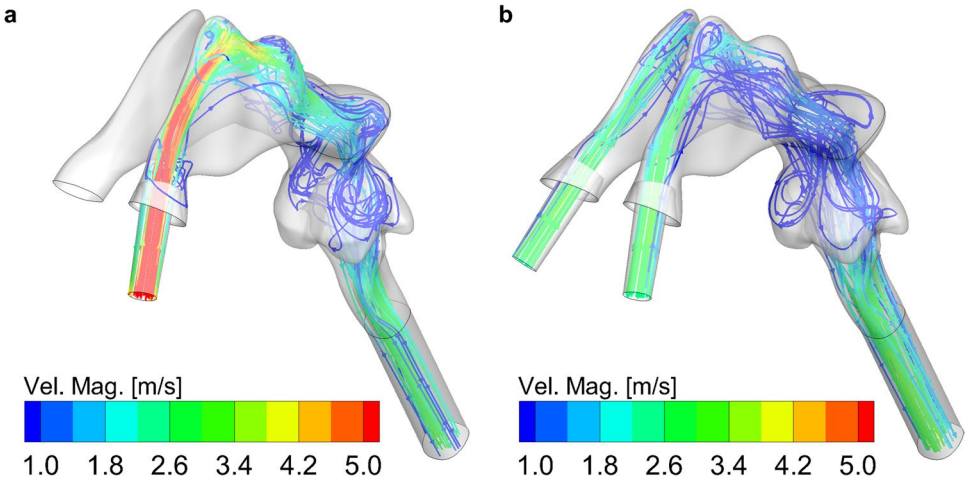

Fig. 4 Comparisons of streamlines through the computational domain between the **a** single and **b** dual external prong cases at a flow rate of 1.85 LPM. Single-prong configurations double the flow rate entering the nasal cavity and cause recirculation zones in the nasopharynx region

(Fig. 4a) and dual (Fig. 4b) prong configurations. The dual-prong configuration reduces the flowrate entering the NT region by half, which is expected to provide a reduction in impaction deposition. The higher intensity air flow in the single-prong case also leads to more chaotic flow behavior through the nasopharyngeal and laryngeal regions, which may be a source of turbulence and increased extrathoracic losses. Based on these observations, it is expected that the dual-prong configuration will reduce deposition from impaction and improve overall aerosol transmission through the NT model. However, the experimental results with external dual prongs indicated higher NT loss compared with the

single-prong case, despite having lower system ED. This trend towards higher dual-prong depositional loss in the experiments is expected to be due to the larger aerosol size exiting the two-outlet dual-prong air-jet device (single prong MMAD = 1.90 (0.1) μm vs. dual prong MMAD = 2.63 (0.12) μm; Table I). CFD simulations will be used to isolate the expected reduction in NT deposition associated with dual prongs when a consistent aerosol size is delivered with both the single- and dual-prong cases.

Comparison Between Models That Include and Exclude the Laryngeal Region

Figure 5 compares deposition patterns and regional NT loss in two models that either include (Fig. 5a) or exclude (Fig. 5b) the larynx for the internal dual-prong configuration with 5-mm insertion depth at a flowrate of 1.85 LPM. The overall deposition fraction (DF_{Tot}) shows only a marginal difference between the two models (28.3% vs. 26.0%) with an absolute difference of approximately 2% and a relative difference of approximately 8%. However, losses in the laryngeal region are very different between the two cases (1.79% vs. 2.53%) with a relative difference of approximately 34%, which is mostly caused by deposition of larger particles (> 8 μm) in the case that includes the larynx. Beyond deposition, the case that includes the larynx provides much higher flow resistance than the model that excludes the larynx (65% relative difference increase), which has an effect on the Euler number and has previously been included in correlations of NT loss in neonates (22).

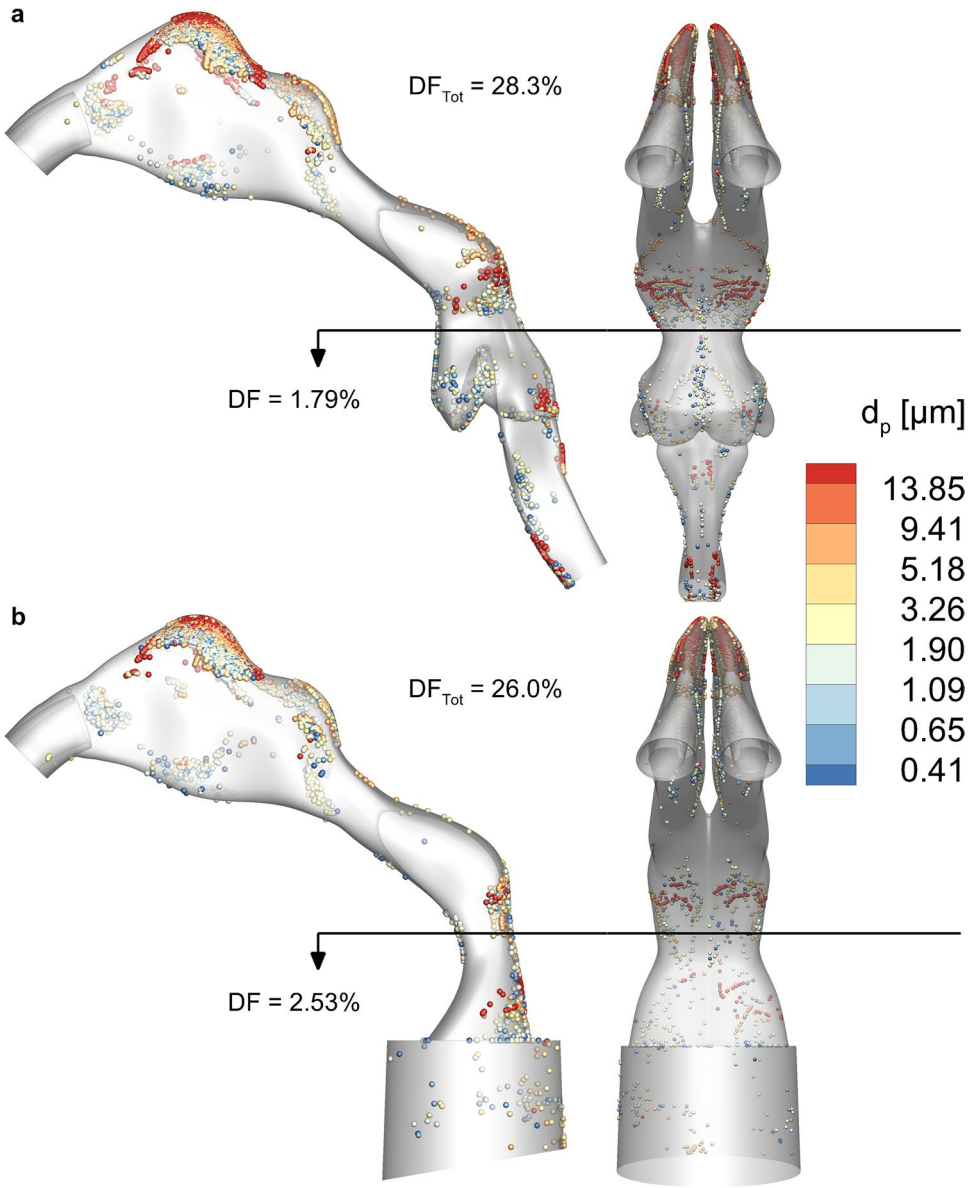

Fig. 5 Profile and frontal views of losses in the dual internal prong with 5 mm insertion cases for NT models that **a** include and **b** do not include a larynx. Overall losses are similar, but regional losses are noticeably different with 34% more loss (relative difference) in the distal region of the nasopharynx in the model that does not include a larynx

Impaction Parameter Curves of Preterm Nose-Throat Loss

Figure 6 plots CFD-predicted NT loss vs. impaction parameter results and the correlation curve for the single-prong configuration with the external prong type (Fig. 6a) and internal prong type at insertion depths of 2 mm (Fig. 6b), 5 mm (Fig. 6c), and 11 mm (Fig. 6d). Similarly, Fig. 7 shows the same plots for the dual-prong configuration. The NT loss is defined as the number of particles that deposit in the NT model divided by the number of particles that enter the domain from the nasal cannula and expressed as a percentage (× 100%). That is, the NT loss does not include deposition in the prongs or upstream losses in the patient interface or device. In both Figs. 6 and 7, the flowrate that is used in the impaction parameter (d_a^2Q) is the device actuation flowrate. The correlations in Figs. 6 and 7 are defined by the following equation and use the parameters that are presented in Table II.

$$\eta = \frac{100}{\left(1 + \exp\left[-kd_a^2Q\right]\right)^a} \tag{1}$$

Table II also presents standard error (SE) and R-squared values for each of the curves in Figs. 6 and 7 to demonstrate the strength of the correlations. In all cases, R-squared shows a strong correlation with values greater than 0.9 and the standard errors are acceptable considering the experimental standard deviation for NT loss can be as high as 6% (see Table I).

The dotted lines on Figs. 6 and 7 compare CFD and correlation predictions of NT loss at a flowrate of 1.4 LPM and particle size of 3.0 µm, which gives an impaction parameter (d_a^2Q) of 12.7 LPM-µm^2. The example here uses a particle size that is often targeted for infant aerosol delivery and the flowrate is based on the peak inhalation flowrate of a preterm infant breathing with a sinusoidal wave form at 50 breaths/min with an inhalation-to-exhalation ratio of 1:1 and tidal volume of 9 mL (6 mL/kg and patient weight of 1.5 kg). Annotations are excluded from the cases with insertion depths of 11 mm (Figs. 6d and 7d), as the CFD results and correlations clearly show increased NT loss across the

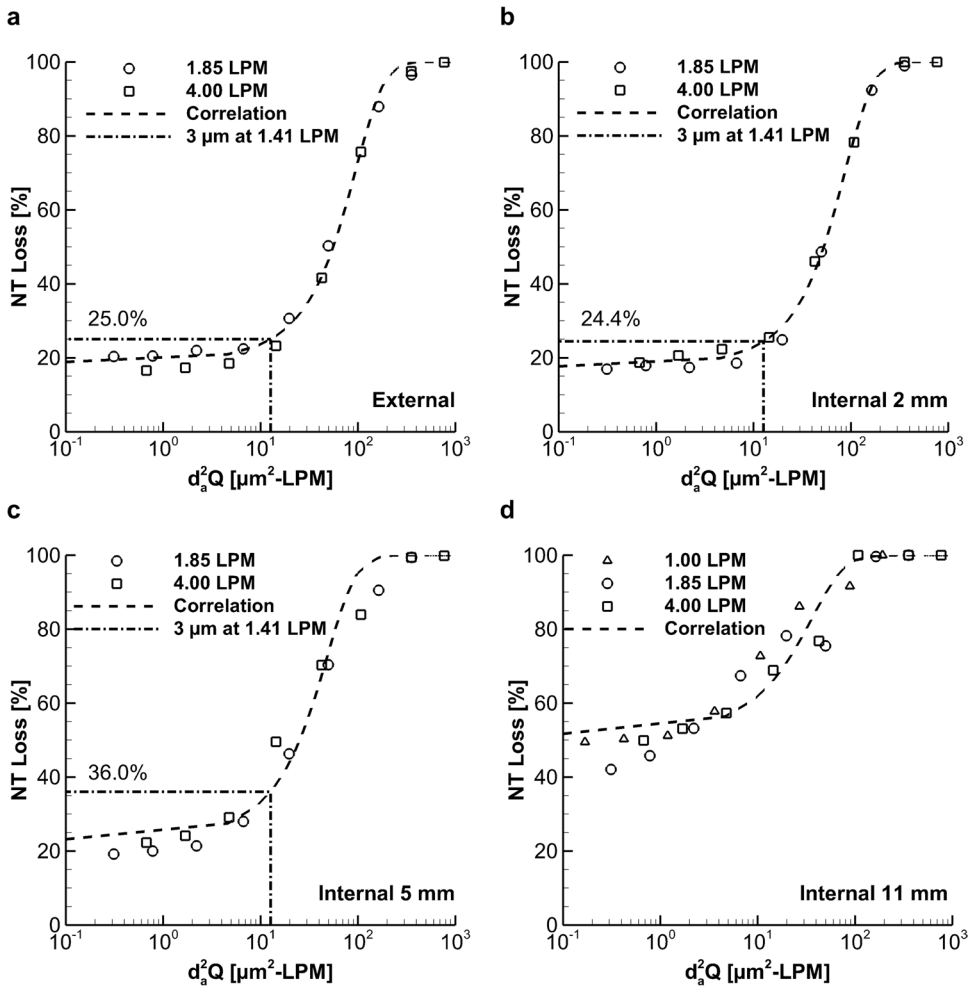

Fig. 6 CFD-predicted impaction parameter curves for the single-prong configuration with the **a** external prong type and internal prong type at insertion depths of **b** 2 mm, **c** 5 mm, and **d** 11 mm. Correlation parameters are given in Table II and defined by Eq. 1. Dash-dot line represent the NT loss (%) for 3 µm particles at a device flow rate of 1.85 LPM

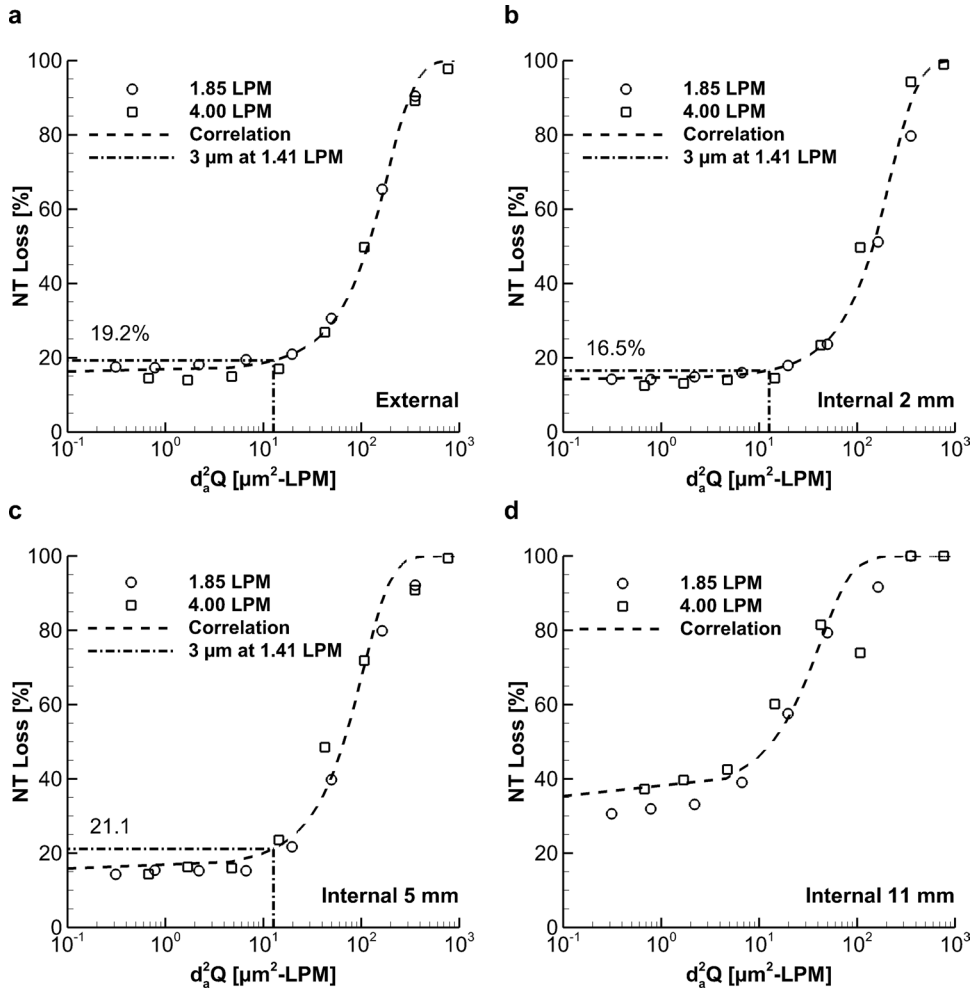

Fig. 7 CFD-predicted impaction parameter curves for the dual-prong configuration with the **a** external prong type and internal prong type at insertion depths of **b** 2 mm, **c** 5 mm, and **d** 11 mm. Correlation parameters are given in Table II and defined by Eq. 1

Table II Summary of Correlation Parameters for the Curves in Figs. 6 and 7 that are Defined with Eq. 1. Standard Error (SE) and *R*-squared Values for each Correlation are also Presented

Prong configuration	Prong type	Insertion depth	*k*	*a*	SE	*R*-squared
Single	External	N/A	0.0197	2.41	2.37	0.9960
	Internal	2 mm	0.0217	2.50	1.74	0.9977
		5 mm	0.0374	2.11	5.66	0.9758
		11 mm	0.0423	0.95	6.15	0.9180
Dual	External	N/A	0.0102	2.62	2.27	0.9959
	Internal	2 mm	0.0088	2.82	4.15	0.9831
		5 mm	0.0182	2.66	5.17	0.9828
		11 mm	0.0389	1.50	7.71	0.9342

SE, standard error

full range of impaction parameter values. At this flowrate and particle size for the single-prong configuration (Fig. 6), the external prong and internal prong with 2-mm insertion perform similarly with expected NT losses of 25.0% and 24.4% respectively. The internal prong with 5-mm insertion depth performs slightly worse with an expected NT loss of 36.0%. For the dual-prong configuration (Fig. 7), the internal prong with 2-mm insertion depth gave the best performance with an expected NT loss of 16.5%. The external prong and internal prong with 5-mm insertion depth both performed slightly worse, with expected NT losses of 19.2% and 21.1% respectively. These results also show that the dual-prong configuration performed better than the single prong for a given prong configuration and particle size such as 16.5%

vs. 24.4% NT loss for the internal prong at 2-mm insertion depth (d_a^2Q of 12.7 LPM-μm^2), which was expected based on evaluation of the flow field in Figs. 3 and 4.

Figure 8 compares the correlations for each of the four cases from the single (Fig. 8a) and dual (Fig. 8b) prong configurations. This figure provides a direct comparison of expected NT losses across a range of impaction parameters for all cases considered in this study. The evaluation of each case discussed above is reinforced by Fig. 8 and shows that a shallower insertion depth for the internal prong type minimizes NT losses by reducing the effect of the jet that enters the nasal cavity on impaction depositional losses.

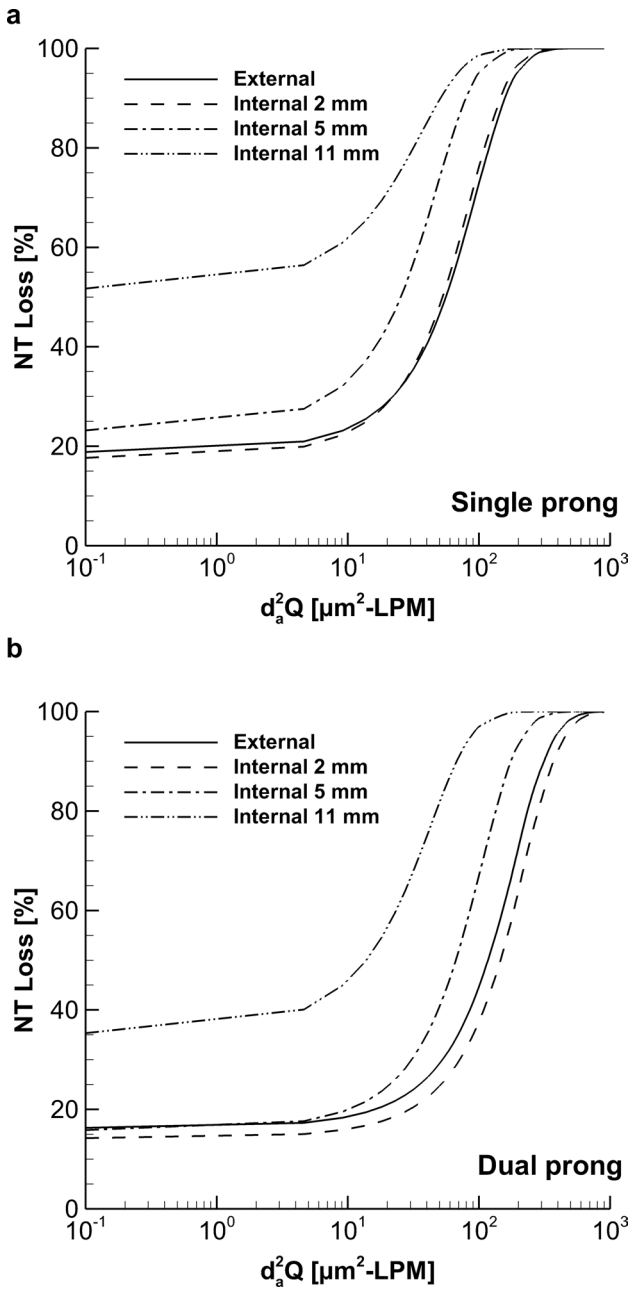

Fig. 8 Comparisons of each impaction parameter correlation for all prong types and insertion depths using the **a** single and **b** dual-prong configurations

Comparison of Nose-Throat Loss Between Cannula Delivery and Ambient Aerosol Inhalation

Figure 9 plots NT loss against the non-dimensional parameters described by Tavernini *et al.* (22) for each of the cases considered in the current study and compares them to experimental correlations of ambient inhalation of aerosols with a neonate model. As with Figs. 6 and 7, the NT loss in Fig. 9 does not include prong losses, which allows direct comparison between the correlations. The correlations in Fig. 9 are defined by the following equation and use the parameters that are presented in Table III.

$$\eta = 1 - \left(\frac{X}{Y + \mathrm{Stk}^{1.2201}\mathrm{Re}^{1.7742}\mathrm{Eu}^{1.5772}} \right)^a \tag{2}$$

Table III also presents standard error (SE) and *R*-squared values for each of the curves in Fig. 9 to demonstrate the strength of the correlations. In all cases, *R*-squared shows a strong correlation with values greater than 0.9 and the standard errors are acceptable. The *a*, *b*, and *c* exponents on the non-dimensional parameter are kept consistent with Tavernini *et al.* (22) to simplify comparisons in Fig. 9, with only the *X* and *Y* correlation parameters adjusted to define new correlations for the results from this study.

The solid curves in Fig. 9 are based on the experimental results from the Tavernini *et al.* (22) study and use average patient-specific values from that article as input to the $\mathrm{Stk}^a\mathrm{Re}^b\mathrm{Eu}^c$ parameter; specifically the characteristic length for Re and the nasal resistance for Eu. Therefore, the solid curve is representative of a typical neonatal model inhaling ambient aerosols, whereas the other curves from the current study are a preterm model inhaling aerosol through a nasal cannula patient interface. This distinction explains the differences that are observed when comparing the expected NT loss curves in Fig. 9. Firstly, inhalation of ambient aerosols shows the potential of 0% NT loss at the lower end of the *S*-curve, whereas inhalation through the cannula prongs shows that best-case NT losses plateau around 15–20%, depending on the configuration. This suggests room for improvement in cannula design that better mimics the introduction of the aerosol into the nasal cavity from ambient inhalation, such as different prong curvature that targets the aerosol through the central path of the middle passage. Approximately 7% of the NT loss from cannula delivery (absolute value) is attributed to transient effects, with some particles dispersed in the continuous phase at the end of device actuation that do not reach the NT model outlet. The remaining 8–13% NT loss with

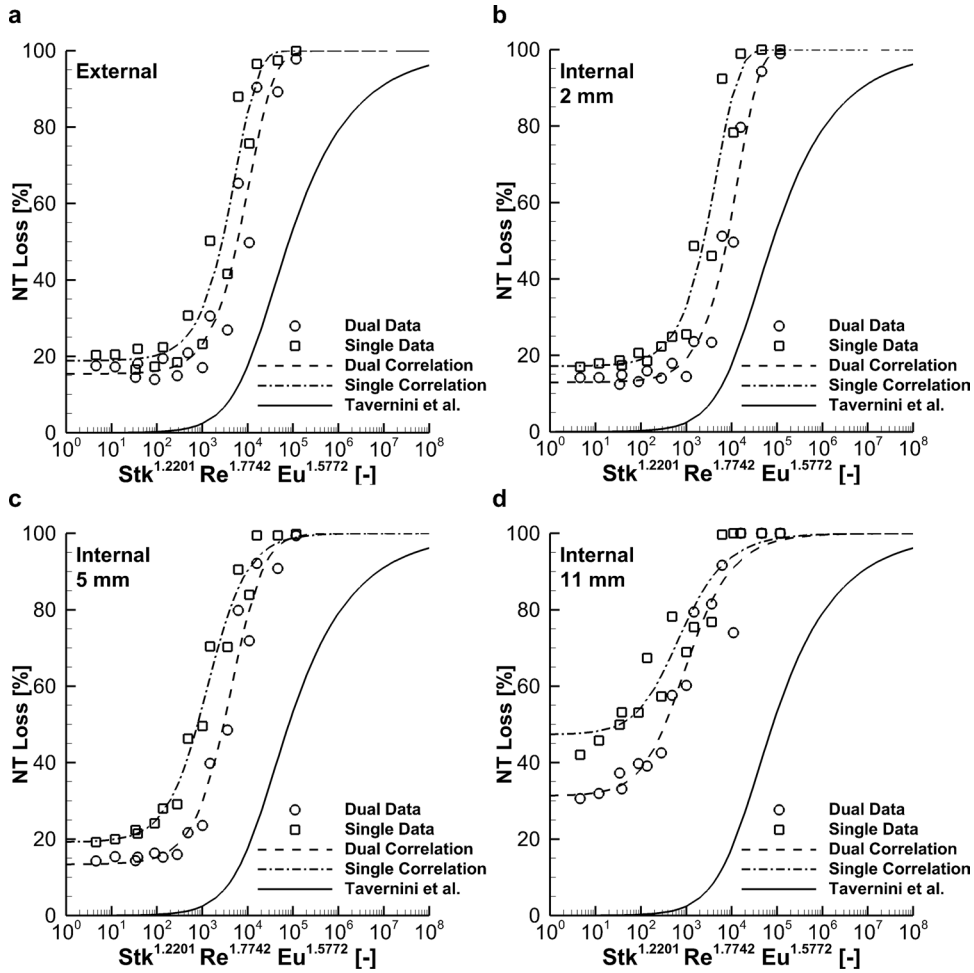

Fig. 9 CFD-predicted comparisons of NT loss between the **a** external prong type and internal prong type at insertion depths of **b** 2 mm, **c** 5 mm, and **d** 11 mm with the experimental correlations from Tavernini *et al.* (22) for ambient inhalation in neonate models. Differences between the cases in this study and the Tavernini *et al.* (22) study are attributed to the inclusion of nasal prongs as opposed to inhaling ambient aerosol. Correlation parameters are given in Table III and defined by Eq. 2

Table III Summary of Correlation Parameters for the Curves in Fig. 9 that are Defined with Eq. 2. Standard Error (SE) and *R*-squared Values for each Correlation are also Presented

Prong configuration	Prong type	Insertion depth	*X*	*Y*	*a*	SE	*R*-squared
Single	External	N/A	34,600	35,700	6.53	8.0	0.9430
	Internal	2 mm	33,300	34,200	7.25	7.2	0.9567
		5 mm	946	1180	0.94	4.7	0.9797
		11 mm	158	415	0.66	6.2	0.9098
Dual	External	N/A	32,200	34,000	3.25	8.1	0.9317
	Internal	2 mm	126,000	128,000	9.28	5.0	0.9746
		5 mm	6730	7350	1.63	5.2	0.9766
		11 mm	336	581	0.68	6.0	0.9511

SE, standard error

cannula delivery is from jet impingement of the aerosol, which can possibly be improved with prong redesigns, and reducing complex flow phenomena like turbulent dispersion. With the best-case difference in NT loss between cannula delivery and ambient aerosol inhalation being 15–20% at the lower end of the *S*-curve, the worst case can be as high as 70 to 80% more NT loss (absolute difference) in the middle range of the $Stk^a Re^b Eu^c$ parameter. This suggests that other delivery methods that are more comparable to ambient inhalation, such as face masks or a hood, may be better than a nasal cannula. However, these methods have their own issues with potential losses on the patient's face, which should be considered when assessing the net loss for the entire system (2, 9, 62, 63). It is also important to remember that the increased NT loss is not as

pronounced when the $Stk^a Re^b Eu^c$ parameter is low, which can be achieved with careful design of the delivery system.

DISCUSSION

This study presented CFD-predicted NT depositional loss curves, based on a validated CFD model and aerosol testing, as a function of impaction parameter ($d_a^2 Q$) for a preterm NT geometry. In all, eight different delivery system configurations were evaluated, with both single- and dual-prong configurations, external and internal prong types, and internal prongs at insertion depths of 2, 5, and 11 mm. Equation 1 combined with the correlation parameters in Table II can be used for any given device flowrate (Q) and aerosol size leaving the cannula prongs (d_a) to estimate the aerosol loss in the preterm NT model with a good degree of accuracy ($r^2 > 0.9$ and standard error ranging from 1.7 to 7.7%). The CFD models that were used to develop these correlations were validated with *in vitro* data for two different prong configurations, which provides confidence in the accuracy of NT loss estimations. The correlations and plots in Figs. 6 and 7 show that the minimum expected NT loss plateaus at approximately 15% for the best design configuration, largely due to the jet effect arising from the prongs and driving aerosol impingement in the nasal cavity.

As a secondary outcome, the NT loss for nasal cannula delivery in preterm patients was compared directly with ambient inhalation of aerosols in neonates (22). This comparison in Fig. 9 shows NT loss as a function of the $Stk^{1.2201} Re^{1.7742} Eu^{1.5772}$ correlation parameter developed by Tavernini *et al.* (22) and further highlights the differences in aerosol transport through the nasal cavity between N2L aerosol administration with a prong configuration and ambient aerosol inhalation. Although the nasal cannula delivery method underperformed when compared to ambient aerosol inhalation, there is potential for the cannula prongs to be redesigned such that they better replicate an ambient aerosol inhalation delivery method. Specifically, the curvature of the prongs can be modified to target delivery through the middle passage of the nasal cavity instead of directing the flow towards impaction sites. Furthermore, the evaluation of the flow field characteristics showed that compression of the internal prongs from a circular to elliptical cross section increased the jet intensity and amplified the impaction deposition loss in the upper region of the preterm NT model. This suggests other aspects of cannula prong design that can be adjusted to minimize NT losses. Finally, as expected, the reduction in flowrate through each nasal passage of the preterm NT model with the dual-prong design leads to a reduction in total NT loss. However, Howe *et al.* (13) reported that the single-prong device design showed improved emitted doses from this air-jet DPI, resulting in an improved net lung delivery of the aerosol. Similar results were found in this study with a different preterm NT in which the decreased aerosolization performance of the air-jet DPI with two outlets resulted in reduced lung delivery efficiency, despite the potential for reduced NT deposition at a specific particle size. These observations can be combined in order to recommend the use of a single-outlet air-jet DPI followed by a bifurcating interface, or the need for improvement in the performance of the two-outlet air-jet design.

The data in Figs. 6 and 7 can be used when designing devices to meet specific performance metrics. For example, if aiming for an acceptable NT loss of < 25%, the target impaction parameters are less than 12.8, 13.8, and 2.0 for the external, internal 2 mm, and internal 5 mm cases, respectively, for the single-prong configuration. Similarly, the target impaction parameters are less than 35.3, 51.6, and 20.9 for the external, internal 2 mm, and internal 5 mm cases, respectively, for the dual-prong configuration. Therefore, for a given device actuation flowrate (Q), the required aerodynamic aerosol size (d_a^2) can be calculated to achieve the target NT loss. This is helpful information in light of the inverse relationship between emitted dose (which closely correlated to actuation flowrate) and outlet MMAD, which was reported in our previous publications on air-jet DPIs (50, 51). Furthermore, if aiming to minimize NT loss, there is a lower limit of impaction parameter, based on the lower end of the *S*-curves in Figs. 6 and 7, below which no further performance improvements are apparent. For example, with the internal prong at an insertion depth of 2 mm, the curve plateaus at the lower end to a NT loss of 17.7% (SE = 1.7%) and 14.2% (SE = 4.2%) for the single- and dual-prong configurations, respectively. This lower limit is due to the jet formation as the flow leaves the cannula and enters the NT region, as illustrated in Fig. 3. There is also little difference in terms of expected NT loss between the single- and dual-prong configurations at the lower end of the *S*-curve, when considering the predicted values and standard error of the correlations, but these differences are more pronounced in the middle region of the curve, as mentioned above with the sample impaction parameter of 12.7 LPM-μm^2.

The main limitation of the current study is the evaluation of only one preterm model to establish predictive correlations of aerosol loss in the NT region. Similar projects in the literature have considered multiple NT models for a given age group (22, 64–67) and have characterized NT loss for a wider population by including interpatient variability. Due to the scarcity of preterm head and neck CT scans, very few models of the preterm NT region are available, which limits evaluation of interpatient variability in this age group. *In vitro* experiments used a flow-through system with filter open to atmosphere. Ideally, a more accurate testing system should include a distal lung analogue configured with

pre-term pulmonary resistance and compliance values. This is necessary to approximate back pressure generated by the DPI in a closed system, which may have shown different results. The lung delivery efficiencies reported are expected to be representative of direct-to-infant delivery strategies where the infant inhales the full aerosol bolus, as with the *in vitro* test conditions considered in this study. Achieving these high lung delivery efficiencies with nCPAP or other forms of NIV will require specially designed interfaces that ensure the infant inhales a majority of the aerosol bolus. Other limitations include the assumptions made with the CFD model related to representation of the flow field and particle trajectories through the NT model. Primarily, hygroscopic growth of the dry powder formulation as it travels through the humid nasal cavity was omitted from the CFD model to improve computational time. However, the residence time of the particles in the NT model is sufficiently small (~ 0.05 s) and airfield relative humidity conditions have not yet reached 99%, such that effects of growth are expected to be minimal in the extrathoracic region. Nevertheless, additional computational and experimental work is needed in this area to ensure correct excipient-enhanced growth aerosol delivery to infants.

As mentioned previously, future work should improve the cannula prong design to maximize nasal transmission and get closer to the levels of NT loss that are observed when inhaling ambient aerosols at low impaction parameter values. Primary design improvements could focus on prong curvature to target the aerosol through the central region of the NT, using rigid material that maintains a circular outlet cross section, and thin prong walls to maximize the outlet area and hence minimize flow velocity. It would also be interesting to evaluate the preterm NT model that was presented in the current study with ambient aerosol delivery to definitively identify whether N2L administration is the only cause of differences between this work and the Tavernini *et al.* (22) data, or if the small scale of the model is the cause for the plateau to approximately 15% at the lower end of the *S*-curve. Future work should also explore improving air-jet DPI performance with two outlet flow passages in order to better facilitate the dual-prong approach. Prong modifications for future evaluation include short rigid geometries, rigid materials, and the use of thin prong walls to minimize the jet effect entering the nose.

CONCLUSIONS

In conclusion, a preterm NT model was characterized for N2L aerosol administration via a nasal cannula with eight different cases, including single- and dual-prong configurations, external and internal prong types, and internal prongs at three insertion depths. The loss in the NT model was evaluated at multiple flowrates and aerosol sizes, with correlations developed for the impaction parameter (d_a^2Q). Comparisons were also made with ambient inhalation of aerosol in neonate models, and the potential for prong design improvements were identified that may minimize NT loss. In the current study, best-case delivery systems suggested NT losses of 15–20% for the dual-prong configuration with external prongs or internal prongs at a 2-mm insertion depth.

Author Contribution Conceptualization, WL, KB; methodology, KB, WL; software, KB; validation, KB, MM, CH, GA, SS; formal analysis, KB, MM, AK, MH, WL; investigation, KB, MM, CH, GA, SS, AK; resources, MM, CH, GA, SS, RD, MH, WL; data curation, KB, MM, CH; writing — original draft preparation, KB, WL, MH; writing — review & editing, WL, MM, AK, MH, RD; visualization, KB, AK, WL; supervision, MH, WL; project administration, MH, WL; funding acquisition, MH, WL.

Funding This work was supported, in whole or in part, by the Bill & Melinda Gates Foundation INV-018833. Under the grant conditions of the Foundation, a Creative Commons Attribution 4.0 Generic License has already been assigned to the author-accepted manuscript version that might arise from this submission.

Data Availability Statement Supporting data are openly available in OSF: https://osf.io/umsfj/?view_only=ca0e1dd442604524bad2828456fd6cbd

Declarations

Conflict of Interest Virginia Commonwealth University is currently pursuing patent protection of devices and methods described in this study, which if licensed and commercialized, may provide a future financial interest to the authors. MH is a member of the Editorial Board of AAPS PharmSciTech.

Open Access This article is licensed under a Creative Commons Attribution 4.0 International License, which permits use, sharing, adaptation, distribution and reproduction in any medium or format, as long as you give appropriate credit to the original author(s) and the source, provide a link to the Creative Commons licence, and indicate if changes were made. The images or other third party material in this article are included in the article's Creative Commons licence, unless indicated otherwise in a credit line to the material. If material is not included in the article's Creative Commons licence and your intended use is not permitted by statutory regulation or exceeds the permitted use, you will need to obtain permission directly from the copyright holder. To view a copy of this licence, visit http://creativecommons.org/licenses/by/4.0/.

References

1. Bhashyam AR, Wolf MT, Marcinkowski AL, Saville A, Thomas K, Carcillo JA, *et al*. Aerosol delivery through nasal cannulas: an in vitro study. J Aerosol Med Pulm Drug Deliv. 2008;21(2):181–7.
2. Fink JB. Delivery of inhaled drugs for infants and small children: a commentary on present and future needs. Clin Ther. 2012;34(11):S36–45.

3. Corcoran TE, Saville A, Adams PS, Johnston DJ, Czachowski MR, Domnina YA, *et al*. Deposition studies of aerosol delivery by nasal cannula to infants. Pediatr Pulmonol. 2019;54(8):1319–25.
4. Sunbul FS, Fink JB, Harwood R, Sheard MM, Zimmerman RD, Ari A. Comparison of HFNC, bubble CPAP and SiPAP on aerosol delivery in neonates: an in-vitro study. Pediatr Pulmonol. 2015;50(11):1099–106.
5. El Taoum KK, Xi J, Kim JW, Berlinski A. In vitro evaluation of aerosols delivered via the nasal route. Respir Care. 2016. https://doi.org/10.4187/respcare.03606.
6. Bianco F, Ricci F, Catozzi C, Murgia X, Schlun M, Bucholski A, *et al*. From bench to bedside: in vitro and in vivo evaluation of a neonate-focused nebulized surfactant delivery strategy. Respir Res. 2019;20(1):134.
7. Bianco F, Salomone F, Milesi I, Murgia X, Bonelli S, Pasini E, *et al*. Aerosol drug delivery to spontaneously-breathing preterm neonates: lessons learned. Respir Res. 2021;22(1):1–31.
8. Réminiac F, Vecellio L, Loughlin RM, Le Pennec D, Cabrera M, Vourc'h NH, *et al*. Nasal high flow nebulization in infants and toddlers: an in vitro and in vivo scintigraphic study. Pediatr Pulmonol. 2017;52(3):337–44.
9. Ari A, Fink JB. Guidelines for aerosol devices in infants, children and adults: which to choose, why and how to achieve effective aerosol therapy. Expert Rev Respir Med. 2011;5(4):561–72.
10. Nord A, Linner R, Salomone F, Bianco F, Ricci F, Murgia X, *et al*. Lung deposition of nebulized surfactant in newborn piglets: nasal CPAP vs nasal IPPV. Pediatr Pulmonol. 2020; 55(2):514–520.
11. Sood BG, Cortez J, Kolli M, Sharma A, Delaney-Black V, Chen X. Aerosolized surfactant in neonatal respiratory distress syndrome: phase I study. Early Human Dev. 2019;134:19–25.
12. Finer NN, Merritt TA, Bernstein G, Job L, Mazela J, Segal R. An open label, pilot study of aerosurf (R) combined with nCPAP to prevent RDS in preterm neonates. J Aerosol Med Pulm Drug Deliv. 2010;23(5):303–9.
13. Howe C, Hindle M, Bonasera S, Rani V, Longest PW. Initial development of an air-jet dry powder inhaler for rapid delivery of pharmaceutical aerosols to infants. J Aerosol Med Pulm Drug Deliv. 2021;34(1):57–70.
14. Pohlmann G, Iwatschenko P, Koch W, Windt H, Rast M, Gama de Abreu M, *et al*. A novel continuous powder aerosolizer (CPA) for inhalative administration of highly concentrated recombinant surfactant protein-C (rSP-C) surfactant to perterm neonates. J Aerosol Med Pulm Drug Deliv. 2013;26(6):370–9.
15. Ruppert C, Kuchenbuch T, Boensch M, Schmidt S, Mathes U, Hillebrand V, *et al*. Dry powder aerosolization of a recombinant surfactant protein-C-based surfactant for inhalative treatment of the acutely inflamed lung. Crit Care Med. 2010;38(7):1584–91.
16. Laube BL, Sharpless G, Shermer C, Sullivan V, Powell K. Deposition of dry powder generated by solovent in Sophia Anatomical infant nose-throat (SAINT) model. Aerosol Sci Technol. 2012;46:514–20.
17. te Pas AB, Walther FJ. A randomized, controlled trial of delivery-room respiratory management in very preterm infants. Pediatrics. 2007;120(2):322–9.
18. Clark A, Newman S, Dasovich N. Mouth and oropharyngeal deposition of pharmaceutical aerosols. J Aerosol Med. 1998;11:S116–20.
19. Storey-Bishoff J, Noga M, Finlay WH. Deposition of micrometer-sized aerosol particles in infant nasal airway replicas. Aerosol Sci. 2008;39:1055–65.
20. Javaheri E, Golshahi L, Finlay W. An idealized geometry that mimics average infant nasal airway deposition. J Aerosol Sci. 2013;55:137–48.
21. Tavernini S, Church TK, Lewis DA, Martin AR, Finlay WH. Scaling an idealized infant nasal airway geometry to mimic inertial filtration of neonatal nasal airways. J Aerosol Sci. 2018;118:14–21.
22. Tavernini S, Church TK, Lewis DA, Noga M, Martin AR, Finlay WH. Deposition of micrometer-sized aerosol particles in neonatal nasal airway replicas. Aerosol Sci Technol. 2018;52(4):407–19.
23. Golshahi L, Finlay WH, Olfert JS, Thompson RB, Noga ML. Deposition of inhaled ultrafine aerosols in replicas of nasal airways of infants. Aerosol Sci Technol. 2010;44:741–52.
24. Zhou Y, Guo M, Xi J, Irshad H, Cheng Y-S. Nasal deposition in infants and children. J Aerosol Med Pulm Drug Deliv. 2014;27(2):110–6.
25. Xi J, Si X, Zhou Y, Kim J, Berlinski A. Growth of nasal and laryngeal airways in children: implications in breathing and inhaled aerosol dynamics. Respir Care. 2014;59(2):263–73.
26. Xi JX, Berlinski A, Zhou Y, Greenberg B, Ou XW. Breathing resistance and ultrafine particle deposition in nasal-laryngeal airways of a newborn, an infant, a child, and an adult. Ann Biomed Eng. 2012;40(12):2579–95.
27. Xi J, Berlinski A, Zhou Y, Greenberg B, Ou X. Breathing resistance and ultrafine particle deposition in nasalâ-laryngeal airways of a newborn, an infant, a child, and an adult. Ann Biomed Eng. 2012;40(12):2579–95.
28. Garcia GJM, Tewksbury EW, Wong BA, Kimbell JS. Interindividual variability in nasal filtration as a function of nasal cavity geometry. J Aerosol Med Pulm Drug Deliv. 2009;22(2):1–17.
29. Golshahi L, Hosseini S. Intranasal filtration of inhaled aerosol in human subjects as a function of nasal pressure drop. J Aerosol Med Pulm Drug Deliv. 2019;32(1):13–23.
30. Clark AR, McKenna C, MacLoughlin R. Aersol delivery in term and preterm infants: the final frontier. Respir Drug Delivery. 2018;2018(1):159–68.
31. Minocchieri S, Burren JM, Bachmann MA, Stern G, Wildhaber J, Buob S, *et al*. Development of the premature infant nose throat-model (PrINT-Model)—an upper airway replica of a premature neonate for the study of aerosol delivery. Pediatr Res. 2008;64(2):141.
32. Youngquist TM, Richardson CP, DiBlasi RM. Effects of condensate in the exhalation limb of neonatal circuits on airway pressure during bubble CPAP. Respir Care. 2013;58(11):1840–6.
33. Janssens HM, de Jongste JC, Fokkens WJ, Robben SG, Wouters K, Tiddens HA. The Sophia Anatomical Infant Nose-Throat (Saint) model: a valuable tool to study aerosol deposition in infants. J Aerosol Med. 2001;14(4):433–41.
34. Bianco F, Pasini E, Nutini M, Murgia X, Stoeckl C, Schlun M, *et al*. Extended pharmacopeial characterization of surfactant aerosols generated by a customized eflow neos nebulizer delivered through neonatal nasal prongs. Pharmaceutics. 2020;12(4):319.
35. Linner R, Perez-de-Sa V, Cunha-Goncalves D. Lung deposition of nebulized surfactant in newborn piglets. Neonatology. 2015;107(4):277–82.
36. Gregory TJ, Irshad H, Chand R, Kuehl PJ. Deposition of aerosolized lucinactant in nonhuman primates. J Aerosol Med Pulm Drug Deliv. 2020;33(1):21–33.
37. Bass K, Boc S, Hindle M, Dodson K, Longest W. High-efficiency nose-to-lung aerosol delivery in an infant: development of a validated computational fluid dynamics method. J Aerosol Med Pulm Drug Deliv. 2019;32(3):132–48.
38. Bass K, Farkas D, Hassan A, Bonasera S, Hindle M, Longest W. High-efficiency dry powder aerosol delivery to children: review and application of new technologies. J Aerosol Sci. 2021;153:105692.
39. Finlay WH, Martin AR. Modeling of aerosol deposition within interface devices. J Aerosol Med. 2007;20(S1):S19–28.
40. Finlay WH, Martin AR. Recent advances in predictive understanding of respiratory tract deposition. J Aerosol Med Pulm Drug Deliv. 2008;21(2):189–205.

41. Delvadia RR, Longest PW, Hindle M, Byron PR. In vitro tests for aerosol deposition. III: Effect of inhaler insertion angle on aerosol deposition. J Aerosol Med Pulm Drug Deliv. 2013;26(3):145–56.
42. Longest PW, Tian G, Walenga RL, Hindle M. Comparing MDI and DPI aerosol deposition using in vitro experiments and a new stochastic individual path (SIP) model of the conducting airways. Pharm Res. 2012;29:1670–88.
43. Longest PW, Hindle M, Das Choudhuri S, Xi J. Comparison of ambient and spray aerosol deposition in a standard induction port and more realistic mouth-throat geometry. J Aerosol Sci. 2008;39(7):572–91.
44. DiBlasi RM, Richardson P. Continuous positive airway pressure. In: Walsh BK, Czervinske MP, DiBlasi RM, editors. Perinatal and Pediatric Respiratory Care. St. Louis: Saunders Elsevier; 2010.
45. Xi, Longest PW, Martonen TB. Effects of the laryngeal jet on nano-and microparticle transport and deposition in an approximate model of the upper tracheobronchial airways. J Appl Physiol. 2008;104(6):1761–77.
46. Schild JA. Relationship of laryngeal dimensions to body size and gestational-age in premature neonates and small infants. Laryngoscope. 1984;94(10):1284–92.
47. Vorperian HK, Kent RD, Lindstrom MJ, Kalina CM, Gentry LR, Yandell BS. Development of vocal tract length during earl childhood: a magnetic resonance imaging study. J Acoust Soc Am. 2005;117(1):338–50.
48. Son Y-J, Longest PW, Tian G, Hindle M. Evaluation and modification of commercial dry powder inhalers for the aerosolization of submicrometer excipient enhanced growth (EEG) formulation. Eur J Pharm Sci. 2013;49:390–9.
49. Howe C, Momin MAM, Farkas D, Bonasera S, Hindle M, Longest PW. Advancement of the infant air-jet dry powder inhaler (DPI): evaluation of different positive-pressure air sources and flow rate. Pharm Res. 2021;38:1615–32.
50. Farkas D, Hindle M, Bass K, Longest PW. Development of an inline dry powder inhaler for oral or trans-nasal aerosol administration to children. J Aerosol Med Pulm Drug Deliv. 2020;33(2):83–98.
51. Longest PW, Farkas D, Bass K, Hindle M. Use of computational fluid dynamics (CFD) dispersion parameters in the development of a new DPI actuated with low air volumes. Pharm Res. 2019;36(8);1–17.
52. Walsh BK, DiBlasi RM. Mechanical ventilation of the neonate and pediatric patient. In: Walsh BK, Czervinske MP, DiBlasi RM, editors. Perinatal and Pediatric Respiratory Care. St. Louis: Saunders Elsevier; 2010. p. 325–47.
53. Thomas ML, Longest PW. Evaluation of the polyhedral mesh style for predicting aerosol deposition in representative models of the conducting airways. J Aerosol Sci. 2022;159:105851.
54. Bass K, Thomas ML, Kemner-van de Corput MPC, Tiddens HAWM, Longest PW. Development of characteristic airway bifurcations in cystic fibrosis. Aerosol Sci Technol. 2021;55(110);1143–1164.
55. Roache PJ. Perspective: A method for uniform reporting of grid refinement studies. J Fluids Eng-Trans Asme. 1994;116(3):405–13.
56. Bass K, Longest PW. Recommendations for simulating microparticle deposition at conditions similar to the upper airways with two-equation turbulence models. J Aerosol Sci. 2018;119:31–50.
57. Wilcox DC. Turbulence modeling for CFD. 2nd ed. California: DCW Industries, Inc.; 1998.
58. Longest PW, Hindle M, Das Choudhuri S, Byron PR. Numerical simulations of capillary aerosol generation: CFD model development and comparisons with experimental data. Aerosol Sci Technol. 2007;41(10):952–73.
59. Longest PW, Vinchurkar S, Martonen TB. Transport and deposition of respiratory aerosols in models of childhood asthma. J Aerosol Sci. 2006;37:1234–57.
60. Walenga RL, Longest PW. Current inhalers deliver very small doses to the lower tracheobronchial airways: assessment of healthy and constricted lungs. J Pharm Sci. 2016;105:147–59.
61. Tian G, Hindle M, Lee S, Longest PW. Validating CFD predictions of pharmaceutical aerosol deposition with in vivo data. Pharm Res. 2015;32:3170–87.
62. DiBlasi RM. Clinical controversies in aerosol therapy for infants and children. Respir Care. 2015;60(6):894–916.
63. Erzinger S, Schueepp KG, Brooks-Wildhaber J, Devadason SG, Wildhaber JH. Facemasks and aerosol delivery in vivo. J Aerosol Med. 2007;20(s1):S78–84.
64. Garcia GJM, Tewksbury EW, Wong BA, Kimbell JS. Interindividual variability in nasal filtration as a function of nasal cavity geometry. J Aerosol Med Pulm Drug Deliv. 2009;22(2):139–55.
65. Golshahi L, Noga ML, Finlay WH. Deposition of inhaled micrometer-sized particles in oropharyngeal airway replicas of children at constant flow rates. J Aerosol Sci. 2012;49:21–31.
66. Golshahi L, Noga ML, Thompson RB, Finlay WH. In vitro deposition measurement of inhaled micrometer-sized particles in extrathoracic airways of children and adolescents during nose breathing. J Aerosol Sci. 2011;42(7):474–88.
67. Storey-Bishoff J, Noga M, Finlay WH. Deposition of micrometer-sized aerosol particles in infant nasal airway replicas. J Aerosol Sci. 2008;39(12):1055–65.

Publisher's Note Springer Nature remains neutral with regard to jurisdictional claims in published maps and institutional affiliations.